Structure and stability of premixed flames stabilized behind the trailing edge of a cylindrical rod at low Lewis numbers

Available online at www.sciencedirect.com

ScienceDirect

Proceedings of the Combustion Institute 35 (2015) 981–988

Proceedings of the Combustion Institute

www.elsevier.com/locate/proci

Structure and stability of premixed flames stabilized behind the trailing edge of a cylindrical rod at low Lewis numbers

V.N. Kurdyumov [a,*], Y.L. Shoshin [b], L.P.H. de Goey [b]

[a] Department of Energy, CIEMAT, Avda. Complutense 40, 28040 Madrid, Spain
[b] Department of Mechanical Engineering, Technische Universiteit Eindhoven, Den Dolech 2, P.O. Box 513, 5600 MB Eindhoven, The Netherlands

Available online 26 June 2014

Abstract

Premixed flames stabilized behind the trailing edge of a semi-infinite cylindrical rod placed coaxially in a circular channel were investigated numerically within the diffusive-thermal model. Apart from the inverted flames, or V-flames, widely reported in the literature, the other kind of flames was observed for the Lewis number lower than unity. The main characteristic of such flames is confinement in the interior of a recirculating vortex formed behind the trailing edge. For a fixed Reynolds number, the flames of this kind exist within a finite range of the Damköhler number. Once the Damköhler number is fixed, they are observed for the Reynolds numbers above a critical value with no limit on large *Re*, assuming that flow remains laminar. Global linear stability analysis of the axisymmetric steady-state solutions of both kinds was performed. The ranges of the parameters where the axisymmetry-breaking bifurcation arises and the oscillatory behavior takes place were found. The results of the stability analysis were successfully compared with the direct two- and three-dimensional numerical simulations.

Keywords: Premixed; Flame stabilization; Burner heat loss

1. Introduction

The stabilization of premixed flames has received much attention in the literature, due to the role it plays in many engineering applications. The earliest studies of stabilized flames anchored on a central bluff-body, or inverted flames, can be traced back to Lewis and von Elbe [1,2]. Such flames resembles the stabilization phenomenon on multiple-slit burners and perforated plates common in industrial and compact household burners.

There have been a number of papers investigating theoretically, experimentally and numerically different stabilization and blow-off mechanisms. Among which one can mention the discussions about the stretch effect [2–4], the flame area increase due to the strong positive curvature at the base flame [5,6], the heat exchange between

* Corresponding author. Fax: +34 91 346 6269.
E-mail address: vadim.k@ciemat.es (V.N. Kurdyumov).

http://dx.doi.org/10.1016/j.proci.2014.05.056
1540-7489/

the flame and the flame-holder [8,7] and the hydrodynamic straining of the flame base [9,10]. Detailed numerical simulations of a methane-air flame stabilized on a perforated plane have been performed recently in [11,12]. Influence of a string stretched along the flow on the stabilization conditions of an inverted propane–air flame was investigated experimentally in [13]. All these studies showed that the stabilization phenomenon comprises a complex nature where a number of physical effects play a role. The latest comprehensive review of the different flame stabilization/blow-off mechanisms can be found in the introductory part of [12].

In the recent article [14], the experimental study of inverted premixed methane–air and hydrogen–methane–air flames stabilized behind the trailing edge of a cylindrical rod positioned along the symmetry axis of the circular channel has been reported. For mixtures with high hydrogen content, anomalous stabilization and blow-off behavior has been observed. Flames in those mixtures could be stabilized at equivalence ratios below the lean flammability limit for a zero-stretch planar flame. Stabilization of such flames was possible only when the mixture velocity exceeded some critical value.

Motivated by the above-mentioned results, the main purpose of the present paper is to elucidate the influence of the differential diffusion effect on flame stabilization. With this aim in view, a constant density approximation is used in order to eliminate the flame–fluid interactions. The problem of the flame attachment is considered for a semi-infinite rod placed coaxially in an infinite circular channel in order to eliminate the external gas entrainment. The steady axisymmetric flames are studied first. A global stability analysis aiming to test the stability properties of the axisymmetric solutions is carried out thereafter. It is followed by the results of the time-dependent dynamics where oscillatory symmetric flames and non-axisymmetric steady flames were obtained. Results of the stability analysis are compared with those of the direct numerical simulations.

2. General formulation

Consider an infinite circular channel with a semi-infinite cylindrical rod positioned along the symmetry axis. The radii of the channel and the rod are R and $R_1 = aR$, respectively, where $a < 1$. A combustible mixture of fuel and oxidizer at initial temperature T_0 flows inside the channel with mass flow rate M. The thermal conductivity of the channel's wall and the rod is taken to be sufficiently high so as to maintain their temperatures constant and equal of the upstream temperature of the mixture T_0. The sketch of the problem and the coordinate system

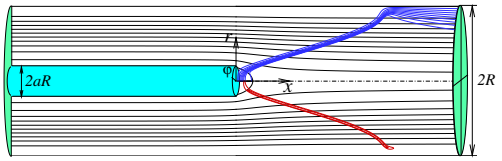

Fig. 1. Sketch of the problem, the coordinate system, illustration of an inverted flame: isotherms (upper half, θ at intervals 0.1), reaction rate contours (lower half, $\omega = 2$ and 10) and stream function contours (ψ at intervals 0.05) calculated for $Le = 1, Re = 100,\ a = 0.2$ and $d = 1500$.

are shown in Fig. 1, where $x = 0$ lies at the head-surface of the rod.

One might imagine conditions, known in the literature as a flashback effect, when a premixed flame propagates upstream in the slot between the rod and the channel's wall. In the opposite situation the flame can be swept away downstream by the flow. In the present work we consider a range of parameters for which a premixed flame is stabilized behind the trailing end of the cylindrical rod. The resulting axisymmetric and non-axisymmetric flames constitute the subject of this paper.

In this study we consider a diffusive-thermal model, formally assuming that the density of the mixture ρ, the thermal diffusivity $\mathcal{D}_T$, the individual molecular diffusivity of fuel $\mathcal{D}$, the heat capacity c_p, and the kinematic viscosity ν are all constant. Consequently, the flow field is not affected by the combustion field and is determined a priori by solving the steady Navier–Stokes equations. If the characteristic length and speed are chosen as R and $U_c = M/\pi\rho R^2$ and the pressure is made dimensionless with respect to the dynamic pressure ρU_c^2, the velocity field $\mathbf{v}$ is determined from

$$(\mathbf{v}\cdot\nabla)\mathbf{v} = -\nabla p + Re^{-1}\nabla^2\mathbf{v}, \qquad \nabla\cdot\mathbf{v} = 0, \qquad (1)$$

where $Re = U_c R/\nu$ is the Reynolds number. It is necessary to stress that, in contrast to the combustion field, the flow field always remains axisymmetric ($\partial/\partial\varphi \equiv 0$), $\mathbf{v} = (u, v)$, where u and v denote the axial and radial velocity components, respectively. Equation (1) was subject to the no-slip condition, $\mathbf{v} = 0$, at all solid surfaces. Anticipating the results presented below, axisymmetry constraint is not required for the temperature and mass fractions fields.

The combustible mixture undergoes a chemical reaction modeled by a global irreversible step $F + O \to P$, where F denotes the fuel, O the oxidizer and P the products. The amount of fuel consumed in moles per unit volume, per unit time, is given by $\Omega \sim \left(\frac{\rho Y_F}{W_F}\right)\left(\frac{\rho Y_O}{W_O}\right)\exp(-E/\mathcal{R}T)$, where Y_F, Y_O are the mass fractions and W_F, W_O are

the molecular weights of the fuel and oxidizer, respectively, ρ is the density of the mixture, E is the overall activation energy, $\mathcal{R}$ is the universal gas constant. Assuming that the mixture is lean in fuel, the oxidizer mass fraction remains nearly constant and $\Omega = \mathcal{B}\rho^2 Y_F \exp(-E/\mathcal{R}T)$, where $\mathcal{B}$ is a pre-exponential factor containing Y_O and the molecular weights. Subindex "F" will not be applied below.

For the sake of a non-dimensional description, it is worth to present the reaction rate in the form

$$\Omega = \rho \frac{U_L^2}{\mathcal{D}_T} \frac{\beta^2}{2Le} Y \exp\left(\frac{E}{\mathcal{R}T_e} - \frac{E}{\mathcal{R}T}\right), \tag{2}$$

where the factor U_L is the asymptotic value of the planar flame speed calculated in the high activation energy limit $\beta \gg 1$, namely $U_L = \sqrt{2\rho\mathcal{B}\mathcal{D}_T Le \beta^{-2}} \exp(-R/\mathcal{R}T_e)$. The temperature $T_e = T_0 + QY_0/c_p$ represents the adiabatic temperature of the planar flame based on the unburned gas temperature T_0, the heat released per unit mass of fuel Q, and the upstream fuel mass fraction Y_0. The non-dimensional value $\beta = E(T_e - T_0)/\mathcal{R}T_e^2$ is the Zel'dovich number.

In the following, we use the laminar flame speed S_L and the thermal flame thickness defined as $\delta_T = \mathcal{D}_T/S_L$ to specify the non-dimensional parameters. The non-dimensional temperature is defined by $\theta = (T - T_0)/(T_e - T_0)$ and the fuel mass fraction is normalized by its upstream value Y_0. By applying Eq. (2) and choosing the convection time R/U_c as a unit of time, the dimensionless transport equations become

$$\frac{\partial\theta}{\partial t} + u\frac{\partial\theta}{\partial x} + v\frac{\partial\theta}{\partial r} = \frac{1}{RePr}\Delta\theta + \frac{d}{RePr}\omega, \tag{3}$$

$$\frac{\partial Y}{\partial t} + u\frac{\partial Y}{\partial x} + v\frac{\partial Y}{\partial r} = \frac{1}{LeRePr}\Delta Y - \frac{d}{RePr}\omega, \tag{4}$$

where $\Delta = \partial^2/\partial x^2 + \partial^2/\partial r^2 + r^{-1}\partial/\partial r + r^{-2}\partial^2/\partial\varphi^2$ is the three-dimensional Laplace operator. The reaction rate ω takes the form

$$\omega = \frac{\beta^2}{2Le\,u_p^2} Y \exp\left\{\frac{\beta(\theta - 1)}{1 + \gamma(\theta - 1)}\right\}. \tag{5}$$

The following non-dimensional parameters appear in the above equations: the Zel'dovich number, $\beta = E(T_e - T_0)/\mathcal{R}T_e^2$, the Lewis number, $Le = \mathcal{D}_T/\mathcal{D}$, the heat release parameter, $\gamma = (T_e - T_0)/T_e$, the Prandtl number, $Pr = \nu/\mathcal{D}_T$, the Reynolds number $Re = M/\pi\rho\nu R$, and the reduced Damköhler number, $d = R^2 S_L^2/\mathcal{D}_T^2$. In the calculations reported below, $\beta = 10$, $\gamma = 0.7$ and $Pr = 0.72$ were assigned. In what follows, these values will be kept fixed considering them as representative for combustion processes.

Equations (3) and (4) are to be solved subject to the following boundary conditions. The function θ and Y are 2π-periodic functions of φ. The solid surfaces are assumed to be impermeable and held at a constant temperature:

$$\theta = 0, \quad \partial Y/\partial n = 0, \tag{6}$$

where $\partial/\partial n$ denotes a normal-surface derivative. Far upstream and far downstream we require

$$x \to -\infty,\ a < r < 1:\ \theta = Y - 1 = 0; \tag{7}$$

$$x \to \infty,\ 0 < r < 1:\ \partial^2\theta/\partial x^2 = \partial^2 Y/\partial x^2 = 0. \tag{8}$$

The numerical simulations reported below showed that the influence of the downstream boundary conditions becomes negligible if the size of the computational domain is sufficiently large. For the axisymmetric calculations, the standard symmetry conditions are required

$$x > 0, \quad r = 0: \quad \partial\theta/\partial r = \partial Y/\partial r = 0, \tag{9}$$

while for three dimension calculations the lack of singularity is required for the temperature and mass fraction fields at the axis.

The factor $u_p = S_L/U_L$ arises in Eq. (5) if the planar flame speed, S_L, is used to define the thermal flame thickness $\delta_T = \mathcal{D}_T/S_L$. Adequate calculation of u_p requires the solution of the eigenvalue problem $d\theta/d\xi = d^2\theta/d\xi^2 + \omega$, $dY/d\xi = Le^{-1}d^2/d\xi^2 - \omega$, with boundary conditions at $\xi \to -\infty: \theta = Y - 1 = 0$, at $\xi \to +\infty: \theta - 1 = Y = 0$, and with ω given by Eq. (5). The numerical values of u_p can be found in [15] as a function of the Lewis number calculated for $\beta = 10$ and $\gamma = 0.7$.

The formulation presented above facilitates to study separately the influence of the fluid dynamics governed by the Reynolds number Re and the effect of the combustion properties of the mixture controlled by the reduced Damköhler number d. These parameters can be easily modified in experiments. Variations in Re are realized by changing the mass flow rate M while parameter d can be modified by means of the equivalent ratio of the mixture which affects directly the planar flame speed S_L. The results presented below elucidate the influence of Re and d on the flame structure for the Lewis number lower then one.

3. Numerical treatment

Steady as well as time-dependent computations were carried out in a finite domain, $x_{min} \leqslant x \leqslant x_{max}$. The typical values were $x_{min} = -0.5$ and $x_{max} = 3.5$, but they were varied to ensure the independence of the results. The spatial derivatives were discretized with second-order, three-point central finite differences on a rectangular uniform grid. The calculations based on the

two-dimensional form of the governing equations (imposing $\partial/\partial\varphi = 0$) were carried out using a typical resolution of $\delta x = \delta r \simeq 0.01$. The number of grid points was doubled in some cases to test the grid independence. When the three dimensions were taken into account, the same accuracy could not be obtained because of computational constraints. Therefore, three-dimensional calculations were made with coarser grids than in the two-dimensional cases, typically using $\delta x = \delta r \simeq 0.02$ and $\delta\varphi \simeq 2\pi/50$. These values were also varied in some cases with no significant influence on the results.

The steady two-dimensional axisymmetric Navier–Stokes Eqs. (1) were written in terms of the stream function ψ defined from the relations $u = r^{-1}\partial\psi/\partial r, v = -r^{-1}\partial\psi/\partial x$ and the vorticity $\zeta = \partial v/\partial x - \partial u/\partial r$. The corresponding equations were solved numerically using a Gauss–Seidel method with over-relaxation.

In order to determine steady (but not necessarily stable) solutions, the steady counterpart ($\partial/\partial t = 0$) of Eqs. (3) and (4) were solved using a Gauss–Seidel method with over-relaxation for two- and three-dimensional cases. For the time-dependent calculations, an explicit marching method was used with first-order discretization in time. A sufficiently small time step $\delta t \sim 10^{-4}$ or less, dictated by the presence of the highly non-linear chemical reaction term (5), was typically chosen to ensure numerical stability. No significant differences were found in the results when δt was halved.

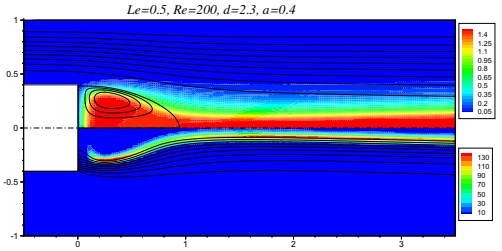

Fig. 2. Inverted flame structure, upper half: temperature distribution (color plot) and stream function contours (ψ at interval 0.05 outside the recirculating region and 0.002 inside); lower half: reaction rate distribution (color plot) and mass fraction contours (Y at interval 0.1); calculated for $Le = 0.5$, $Re = 200$, $a = 0.4$ and $d = 2.3$.

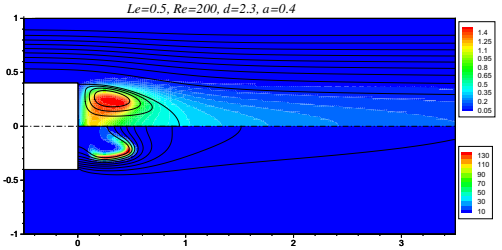

Fig. 3. Vortex flame structure, upper half: temperature distribution (color plot) and stream function contours (ψ at interval 0.05 outside the recirculating region and 0.002 inside); lower half: reaction rate distribution (color plot) and mass fraction contours (Y at interval 0.1); calculated for $Le = 0.5$, $Re = 200, a = 0.4$ and $d = 2.3$.

4. Axisymmetric steady-state flames

Consider first the steady axisymmetric counterpart ($\partial/\partial t = \partial/\partial\varphi = 0$) of Eqs. (3), (4). The numerical calculations of the corresponding two-dimensional equations showed existence of two kinds of solutions with qualitatively different temperature and reaction rate distributions. The first kind of solutions comprises the inverted flames widely investigated experimentally and numerically in the past. Such a flame, exemplified in Fig. 1, consists of the edge situated immediately behind the rod and the cone-like flame extending downstream. When d is sufficiently large, the cone angle remains notable and the flame approaches to the channel wall, as shown in Fig. 1. With decreasing values of d (for a fixed value of Re) the flame cone shrinks being transformed into a cylindrical flame tail surrounding the axis, as shown in Fig. 2. It should be noted that flames with a cylindrical tail also belong among the inverted flame family because they can be obtained from them by gradual reduction of d. Hence we will refer to these flames as the "inverted" flames.

The other kind of flames found numerically is shown in Fig. 3 calculated for $Le = 0.5$, $a = 0.4$, $Re = 200$ and $d = 2.3$. One can see that this flame is confined entirely inside the recirculating region formed behind the rod with no flame prolonged in the rear. The lack of the flame tail is considered below as a main characteristic of these flames. This kind of flames is referred to below as the "vortex" flames. It is necessary to stress that the flames shown in Figs. 2 and 3 were obtained at exactly the same set of parameters.

In order to characterize a flame quantitatively, the dimensionless total heat flux into the rod is introduced in the form

$$q = 2\pi a \int_{-\infty}^{0} \frac{\partial\theta}{\partial r}|_{r=a}\, dx + 2\pi \int_{0}^{a} \frac{\partial\theta}{\partial x}|_{x=0}\, r\, dr. \qquad (10)$$

This quantity computed for flames with $Le = 0.5$ is plotted in Fig. 4 as a function of the reduced Damköhler number d for various values of the Reynolds number Re and $a = 0.4$. The curves corresponding to the inverted and vortex flames are plotted with solid and dashed lines, respectively. The flame extinction points of the inverted flame are marked in this figure with gradient symbols while the critical points of vortex flames are marked with circles.

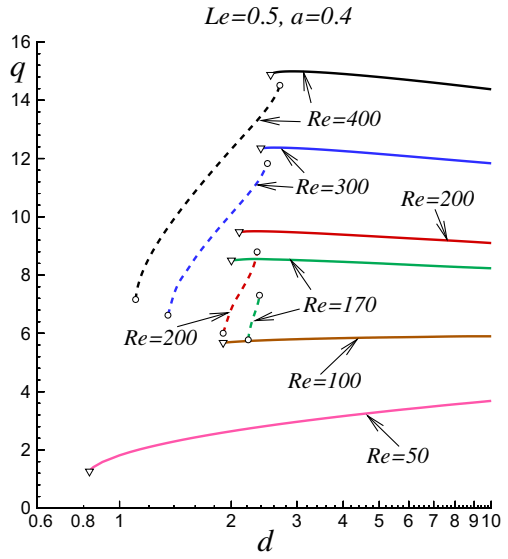

Fig. 4. Response curves showing the dependence of the total heat flux to the rod given by Eq. (10) as a function of the reduced Damköhler number d, for several values of the Reynolds number. The solid segments correspond to the inverted flames, the dashed segments to vortex flames, the circles and gradient symbols show the extinction points.

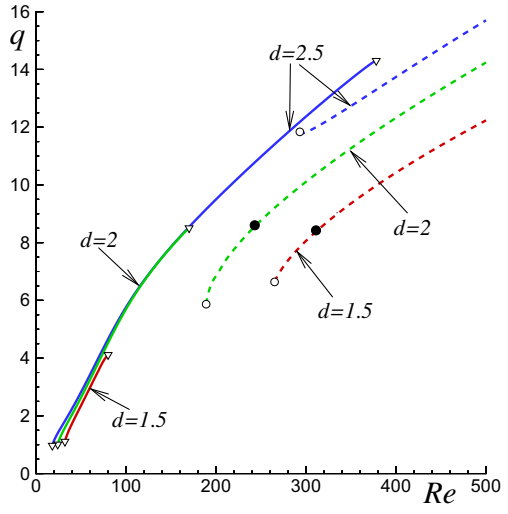

Fig. 5. Response curves showing the dependence of the total heat flux to the rod given by Eq. (10) as a function of the Reynolds number Re, for several values of the reduced Damköhler number d. The solid segments correspond to the inverted flames, the dashed segments to vortex flames, the circles and gradient symbols show the extinction points and the black-filled circles (•) mark the marginally stable states ($n = 1$) of the vortex flames for $d = 1.5$ and $d = 2$.

One can see in Fig. 4 that when the Reynolds number is larger than a critical value, $Re > Re_c$, the vortex flames (dashed lines) exist within a finite range of the reduced Damköhler number, $d_{min} < d < d_{max}$. No vortex flames were found for $Re < Re_c$. In contrast to this, the inverted flames (solid lines) exist for $d > d_c$ and no limit on d was found for $d > d_c$ for a fixed value of Re. The critical Reynolds number above which the vortex flames can be observed was found about $Re_c \approx 165$ computed for $Le = 0.5$ and $a = 0.4$.

In Fig. 5 the heat flux q is shown as a function of the Reynolds number Re for the values of the reduced Damköhler number equal to 1.5, 2 and 2.5. All curves were calculated for $Le = 0.5$ and $a = 0.4$. The solid curves correspond to the inverted flames and the dashed ones to the vortex flames. The critical points of the vortex flames are indicated with circles and the critical point of the inverted flames are shown with gradient symbols.

Figure 5 shows that for small values of d the inverted flames exist within a finite interval of Re (bounded by the gradient symbols). This interval widens for increasing values of the Damköhler number becoming unbounded for high Reynolds numbers for sufficiently large d. Figure 5 shows also that the vortex flames exist for the Reynolds numbers larger than a critical value. It is interesting, that for sufficiently small d (e.g. case with $d = 1.5$) the existence regions of the inverted and vortex flames are separated by an interval of d with no flames.

All these results are summarized in Fig. 6 where the curves bounding the existence regions of the inverted and vortex flames are shown for $Le = 0.5$ and $a = 0.4$. The critical curve corresponding to the inverted flames is plotted with a solid line and gradient symbols while the curve of the vortex flames is shown with a dashed line with circles. The inverted flames exist in the region above the solid curve and the vortex flame appear to the right of the dashed curve. It is interesting that there is a region where both kinds of flames coexist. The flames from this region are shown in Figs. 2 and 3 computed for the values marked with a dark point in Fig. 6, namely $Re = 200$ and $d = 2.3$.

5. Stability analysis

Global stability analysis of the axisymmetric steady-states presented in the previous section is described below. Two-dimensional distributions of the steady-state temperature and mass fraction, all now denoted by subindex "0", are perturbed as usual with small perturbations

$$\theta = \theta_0(x,r) + \epsilon F(x,r)\exp(\lambda t + in\varphi),$$
$$Y = Y_0(x,r) + \epsilon G(x,r)\exp(\lambda t + in\varphi), \qquad (11)$$

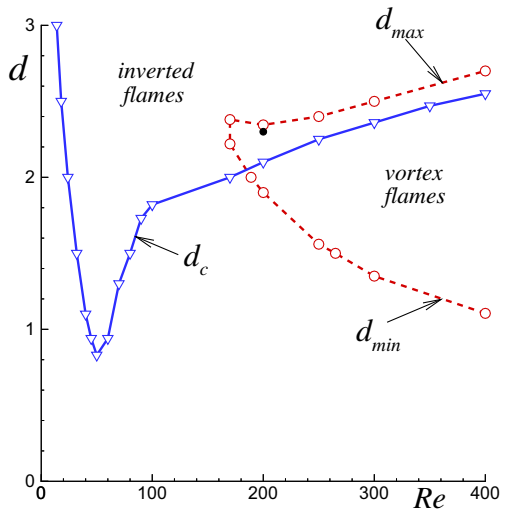

Fig. 6. Existence diagram in Re–d plane for $Le = 0.5$, $d = 0.4$. Vortex flames exist to the right of the dashed curve with circles; inverted flame exist above the solid curve with gradient symbols. Black-filled circle indicates the flames shown in Fig. 2 and 3.

where $\epsilon \ll 1$ is the perturbation amplitude, λ is a complex number, $n = 0, 1, 2\ldots$ is the azimuthal wave number where the mode with $n = 0$ represents axisymmetric perturbation. The real part of λ gives the growth rate. The linearized eigenvalue problem obtaining when substituting Eq. (11) into Eqs. (3), (4) takes the form

$$\lambda F + uF_x + vF_r = \left\{\hat{\mathcal{L}}F + AF + BG\right\}/RePr,$$
$$\lambda G + uG_x + vG_r = \left\{Le^{-1}\hat{\mathcal{L}}G - AF - BG\right\}/RePr, \tag{12}$$

where $\hat{\mathcal{L}} = \partial^2/\partial x^2 + \partial^2/\partial r^2 + r^{-1}\partial/\partial r - n^2 r^{-2}$. The functions A and B appearing in Eqs. (12) are all functions of x and r determined by the steady-state solution

$$A = \frac{d\beta^3 Y_0}{2Leu_p^2[1+\gamma(\theta_0-1)]^2}\exp\left\{\frac{\beta(\theta_0-1)}{1+\gamma(\theta_0-1)}\right\},$$
$$B = \frac{d\beta^2}{2Leu_p^2}\exp\left\{\frac{\beta(\theta_0-1)}{1+\gamma(\theta_0-1)}\right\}$$

The appropriate boundary conditions are

$$F = \partial G/\partial n = 0 \tag{13}$$

at the solid surfaces and

$$x \to -\infty: F = G = 0$$
$$x \to \infty: \partial^2 F/\partial x^2 = \partial^2 G/\partial x^2 = 0 \tag{14}$$

far upstream and downstream. It can be shown that at the axis of the channel the following condition should be imposed

$$r = 0, x > 0: \begin{array}{l} \partial F/\partial r = \partial G/\partial r = 0, n = 0; \\ F = G = 0, n > 0. \end{array} \tag{15}$$

The eigenvalue problem given by Eqs. (12)–(15) is not amenable to the analytical analysis and, therefore, numerical calculations are required. The numerical method described in [15] was applied to calculate the eigenvalue with a greatest real part, or the main eigenvalue. This eigenvalue determines completely if a given steady-state is stable or not. If the real part of this eigenvalue is positive, $\lambda_R > 0$, then the steady-state is unstable, and, conversely, if its real part is non positive, $\lambda_R \leqslant 0$, the steady-state is linearly stable.

Consider first the stability of vortex flames shown by dashed response curves in Fig. 5. The growth rate λ_R is shown in Fig. 7 as a function of the Reynolds number for the modes with the azimuthal wave-numbers $n = 0, 1$ and 2, all calculated with $Le = 0.5$, $d = 1.5$. The solid and dashed segments in Fig. 7 correspond to the eigenvalues with zero and non-zero imaginary part, respectively. The extinction point is indicated with the symbol ○. One can see that when the Reynolds number decreases below a critical value, marked in Fig. 7 with the symbol •, the eigenvalue corresponding to the $n = 1$ mode becomes positive. This critical point is shown with the same symbol in Fig. 5 for $d = 1.5$ and 2. With decreasing Re even further, the eigenvalue corresponding to the next mode, $n = 2$, also becomes positive. Notice that the $n = 1, 2$ eigenvalues are both real. The axisymmetric mode $n = 0$ is also plotted in

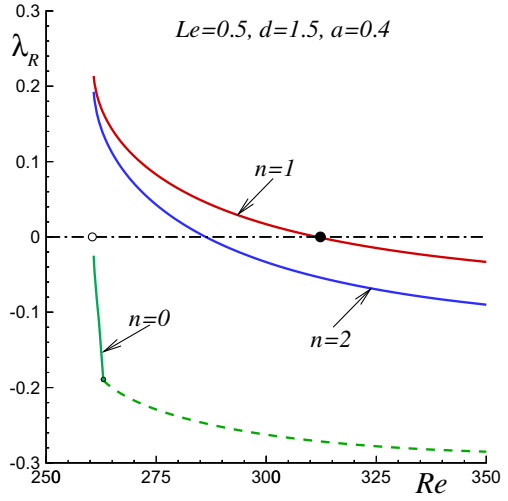

Fig. 7. The growth rate λ_R as a function of the Reynolds number for several modes, computed for the symmetric vortex flame with $Le = 0.5$, $a = 0.4$; the solid segments correspond to $\lambda_I = 0$, the dashed segment to $\lambda_I \neq 0$, a black-filled circle (•) to marginally stable state, and a circle (○) to extinction state.

Fig. 7 having $\lambda_I \neq 0$ for sufficiently large Re and becoming completely real near the extinction point. It is important that for the axisymmetric mode $n = 0$ the real part remains negative and the $n = 0$ mode is stable. The numerical calculations showed that for the eigenvalues with $n > 2$ (not plotted) $\lambda_R < 0$ and these perturbation modes also remain stable. It was found also that the growth rate λ_R calculated for the $n = 1,\ 2$ modes remain always negative for higher value of d and the axisymmetric flames corresponding to the dashed curve calculated with $d = 2.5$ are all stable.

The results of the global stability analysis of the axisymmetric vortex flame indicate that the flame loses stability for sufficiently low values of Re and d near the extinction limit. One can expect that, because of $\lambda_R > 0$ and $\lambda_I = 0$ for $n = 1, 2$, this loss of stability produces a flame which is non-axisymmetric and time-independent, by analogy with the cellular instability of planar flames. The direct numerical calculations based on the three-dimensional Eqs. (3), (4) reinforce the stability results. Figure 8 shows the iso-surface of the constant temperature $\theta = 0.5$ plotted for the steady-state 3D-solution calculated with $Re = 270,\ Le = 0.5$ and $a = 0.4$.

Consider now the stability of the inverted flames represented in Fig. 5 with solid curves. This figure shows that for low values of d the inverted flame exist within a finite interval of the Reynolds number, $Re_{min} < Re < Re_{max}$. In Fig. 9 we plot the dependence of the real part of the eigenvalue λ_R on the Reynolds number for the perturbation modes $n = 0$ and $n = 1$ calculated with $d = 1.5$, $Le = 0.5$ and $a = 0.4$. One can see that apart from a tiny interval close to Re_{max} the axisymmetric inverted flame remains stable. With Re approaching to R_{max} the Hopf bifurcation occurs for the

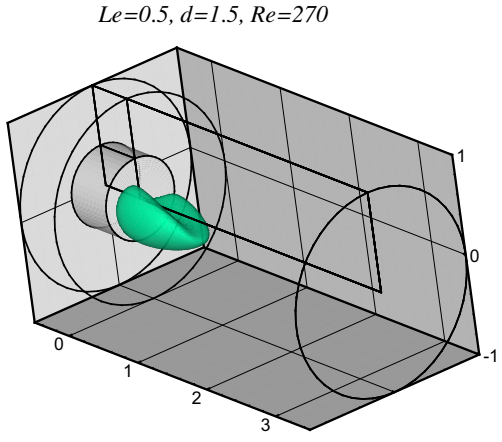

Fig. 8. Three-dimensional iso-surface $\theta = 0.5$ calculated for the non-axisymmetric vortex flame with $Le = 0.5$ and $a = 0.4$.

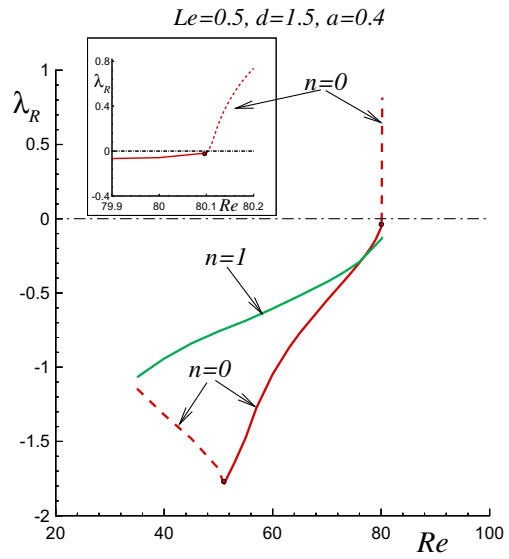

Fig. 9. The growth rate λ_R as a function of the Reynolds number for $n = 0$ and $n = 1$ modes, computed for the symmetric inverted flame with $Le = 0.5,\ a = 0.4$; the solid segments correspond to $\lambda_I = 0$, the dashed segment to $\lambda_I \neq 0$.

axisymmetric mode $n = 0$ and the real part of the eigenvalue becomes positive. It is important that all non-axisymmetric modes ($n > 0$) remain stable having $\lambda_R > 0$.

This fact makes possible to use the two-dimensional counterpart of Eqs. (3), (4). The calculations were carried out for $Le = 0.5$ and the Reynolds number close to Re_{max}. In Fig. 10 we show the time history of the temperature maximum in the domain for distinct Re. One can see that for $Re = 79$ the flame is stabilized after a transitory time while for the case with $Re = 80.2$ the maximum temperature suffers oscillations with a constant amplitude. Finally, for $Re = 80.5$, the extinction event takes place. Apparently there will exist difficulties to observe such oscillatory behavior in experiments due to the range of the Reynolds number is very narrow.

6. Conclusions

In this study, we have examined numerically the structure and stability of the flames formed behind the trailing edge of a cylindrical rod placed coaxially in a circular channel. The flame stabilization occurs due to the low flow velocity region behind the rod. In the analysis we suppressed hydrodynamic disturbances, but relying on a realistic flow field computed from the full Navier–Stokes equations. The existence of two kinds of flames has been demonstrated for the Lewis

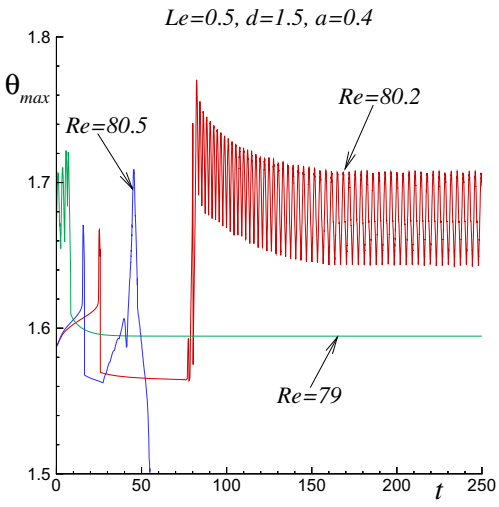

Fig. 10. Temporal variations of the maximum temperature for different Re, calculated for $Le = 0.5$ and $a = 0.4$.

number lower than one. The first kind of flames comprises the well-known V-flame family for which the low flow-velocity region formed immediately behind the trailing edge plays a role of a flame holder and the flame extends downstream in the form of a cone or a cylinder.

The second kind of flames has a completely different structure. The distinctive property of these flames, denominated in the paper as the vortex flames, is to be confined inside the recirculating region. Evidently, the vortex flames can exist only if the characteristic size of the recirculating region is sufficiently large. The other requisite condition is the Lewis number lower than one. It is interesting that two kinds of fames can coexist for some values of parameters. The loss stability of the axisymmetric flames of both kinds was studied by means of the global stability analysis and direct numerical simulations. It was found that the axisymmetric inverted flame can manifest an oscillatory behavior while the axisymmetric vortex flames can turn into a non-axisymmetric flames close to the extinction limits.

Acknowledgments

V.K. acknowledges the support of Spanish MEC under projects #ENE2011–27686-C02–01 and #CSD2011–0001 and Y.Sh. acknowledges the financial support of the Dutch Technology Foundation (STW), Project 11616.

Appendix A. Supplementary data

Supplementary data associated with this article can be found, in the online version, at http://dx.doi.org/10.1016/j.proci.2014.05.056.

References

[1] B. Lewis, G. von Elbe, *J. Chem. Phys.* 11 (1943) 75–97.
[2] B. Lewis, G. von Elbe, *Combustion, Flames and Explosions of Gases*, Academic Press, New York, 1961.
[3] H. Edminson, M.P. Heap, *Combust. Flame* 14 (1970) 191–194.
[4] S.B. Reed, *Combust. Flame* 11 (1967) 75–97.
[5] T. Kawamura, K. Asato, T. Mazaki, T. Hamaguchi, H. Kayahara, *Combust. Flame* 35 (1979) 109–116.
[6] T. Kawamura, K. Asato, T. Mazaki, *Combust. Flame* 45 (1982) 225–233.
[7] C.J. Sung, C.K. Law, A. Umemura, *Proc. Combust. Inst.* 24 (1992) 205–212.
[8] C. Treviño, S. Donnerhack, N. Peters, *Combust. Flame* 85 (1992) 505–5010.
[9] R.M.M. Mallens, B.O. Loijenga, L.P.H. de Goey, P.J.M. Sonnemans, *Combust. Sci. Technol.* 122 (1997) 331–344.
[10] R.M.M. Mallens, L.P.H. de Goey, C.K. Law, *Combust. Sci. Technol.* 159 (2000) 373–389.
[11] H.M. Altay, K.S. Kedia, R.L. Speth, A.F. Ghoniem, *Combust. Theory Model.* 14 (2010) 125–154.
[12] K.S. Kedia, A.F. Ghoniem, *Combust. Flame* 159 (2012) 1055–1069.
[13] M.M. Alekseev, V.P. Samsonov, *Combust. Explosion Shock Waves* 45 (2009) 111–118.
[14] Y. Shoshin, R.J.M. Bastiaans, L.P.H. de Goey, *Combust. Flame* 160 (2013) 565–576.
[15] V.N. Kurdyumov, *Combust. Flame* 158 (2011) 1307–1317.